ACS APPLIED MATERIALS & INTERFACES

Research Article

www.acsami.org

Flexible Free-Standing Graphene/SnO_2 Nanocomposites Paper for Li-Ion Battery

Junfei Liang, Yue Zhao, Lin Guo,* and Lidong Li*

School of Chemistry and Environment, Beihang University, Beijing, 100191, P. R. of China

Supporting Information

ABSTRACT: A flexible free-standing graphene/SnO_2 nanocomposites paper (GSP) was prepared by coupling a simple filtration method and a thermal reduction together for the first time. Compared with the pure SnO_2 nanoparticles, the GSP exhibited a better cycling stability, because the graphene with high mechanical strength and elasticity can work as a buffer to prevent the volume expansion and contraction of SnO_2 nanoparticles during the Li^+ insertion/extraction process. Meanwhile, compared with single graphene paper, the GSP showed a higher capacity because of the hybridizing with higher capacity SnO_2 nanoparticles. The excellent electrochemical performance of the GSP as an anode material in Li-ion battery was obtained. The as-prepared GSP shows a great potential for flexible Li-ion batteries.

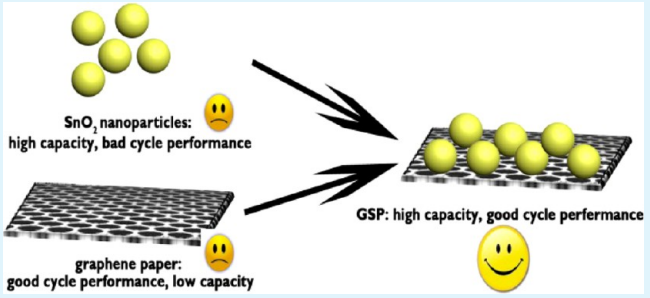

KEYWORDS: *flexible, free-standing, GSP, Li-ion battery, cycling stability, capacity*

1. INTRODUCTION

Modern electronic devices such as mobile communication devices, portable electronic, devices and electric/hybrid vehicles require high-performance batteries to power them.[1] The Li-ion battery is one of the most suitable candidates to satisfy the requirements because it has high energy density and high voltage and is lightweight. Among various Li-ion batteries, the flexible Li-ion battery holds great promise for rollup displays, smart electronics, wearable devices, and other applications.[2,3] There has been a strong market demand for the flexible Li-ion battery. Their large-scale use, however, is mainly limited by our capability to fabricate flexible Li-ion electrodes. One useful strategy to circumvent this difficulty is to fabricate flexible Li-ion electrodes by mixing particulate electrode materials with polymer binders and conductive agents and then coating the mixtures on a flexible substrate.[4] However, this method is complicated and time-consuming. Most materials used to make flexible substrates are unstable under the electrodes fabrication process. This is mainly due to the lack of a reliable material that combines electronically superior conductivity, high mechanical flexibility, and high stability in electrochemical environments.[4,5]

Graphene, a one-atom thick and two-dimensional closely packed honeycomb lattice, has received numerous investigations from both the experimental and theoretical scientific communities since the experimental observation of single layer by K. S. Novoselov and A. K. Geim in 2004.[6] Graphene exhibits a number of intriguing properties, such as excellent intrinsic carrier mobility (~200 000 $cm^2/V{\cdot}s$),[7] quantum electronic transport,[8,9] high mechanical strength and elasticity,[10] superior thermal conductivity,[11] chemical stability within a wide range of electrochemical potentials, and so on.[5] In addition, recent studies have shown that graphene nanosheets can be easily fabricated in large quantities through chemical conversion from commercially available, inexpensive graphite[12−14] and the graphene nanosheets can be facilely assembled into flexible paper-like materials through flow-directed assembly by a simple vacuum filtration of their colloidal dispersions.[15,16] In particular, free-standing graphene paper outperforms many other paper-like materials, such as carbon nanotubes (CNT) paper or graphite foil in mechanical stiffness and strength. On the basis of so many extraordinary properties mentioned above, we expected to see that the free-standing graphene paper may become a reliable material that could be used for the flexible Li-ion battery. However, when using the graphene paper as an anode material for Li-ion batteries, their capacities are very low (only around 100 mAh/g) although they show a good cycling stability, which indicates that the graphene paper itself is not suitable for the application as the anode material in secondary or rechargeable Li-ion batteries.[17] Incorporating an electrochemically active second phase with higher capacity into the graphene paper is a practical way to improve the capacity of the free-standing graphene paper in Li-ion batteries.

SnO_2, as an ideal anode material to replace currently used graphite for next generation Li-ion batteries, has attracted much attention because of its high theoretical reversible Li^+ storage capacity (calculated to be 782 mAh/g) and its low discharge potential.[18] However, the practical application of SnO_2 as anode is hampered by its poor cycle performance, resulting

Received: June 11, 2012
Accepted: October 22, 2012
Published: October 22, 2012

   dx.doi.org/10.1021/am301962d | ACS Appl. Mater. Interfaces 2012, 4, 5742−5748

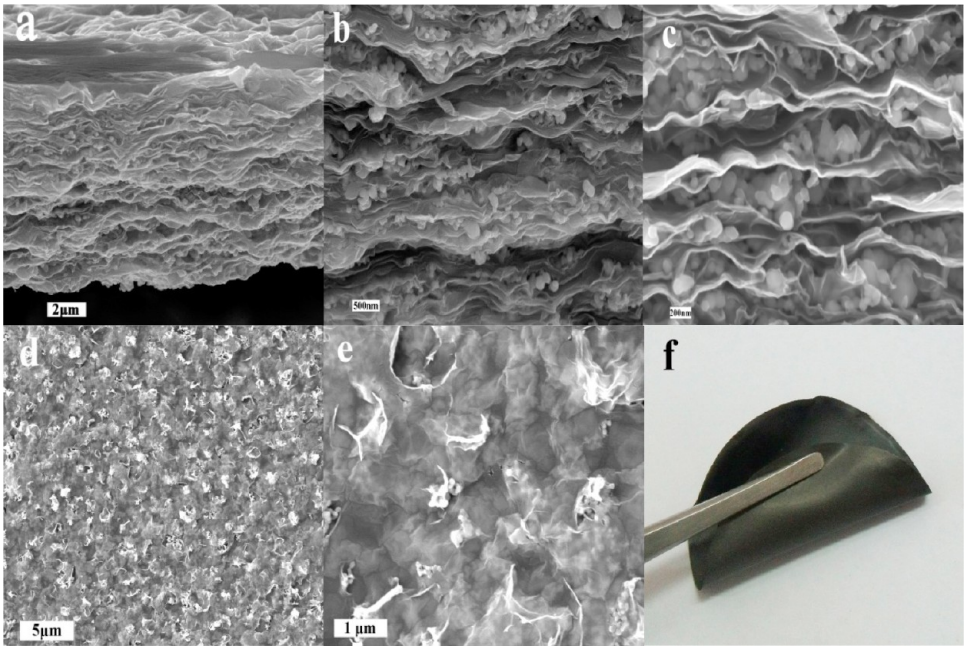

Figure 1. (a–c) Low-, middle-, and high-resolution FESEM cross section images of the paper; (d, e) low and high magnification FESEM top view images of the paper; (f) photograph of the as-prepared GOSP.

from the serious volume expansion and contraction (up to about 300%) during the insertion and extraction processes of Li^+.[19,20] To solve this problem, various methods have been tested.[19−27] Results have shown that hybridizing SnO_2 with carbon materials is an effective method to accommodate the strain of volume change during the charge/discharge process.[26−30] Up to date, there have been a lot of reports of the preparation of graphene/SnO_2 nanocomposites and those nanocomposites showed better Li-storage performance.[31−45] However, to our best knowledge, there are only a few people reporting the use of a flexible free-standing graphene/SnO_2 nanocomposite for Li-ion battery. Wang and his collaborators prepared a free-standing graphene/SnO_2 nanocomposites film Li-ion battery.[32] However, the process to prepare the film was complicated and time-consuming, and the film only showed a good performance in a low current density (under 20 mA/g).

In this paper, we first prepared a flexible free-standing graphene/SnO_2 nanocomposites paper (GSP) by a simple filtration method together with a thermal reduction. Compared with single graphene paper, the GSP showed a higher capacity because of the hybridizing with higher capacity of SnO_2 nanoparticles. Meanwhile, compared with the pure SnO_2 nanoparticles, the GSP exhibited a better cycling stability because of the hybridizing with graphene which has excellent mechanical strength and elasticity, high surface area, and superior electronic conductivity. The excellent mechanical strength and elasticity of graphene nanosheets permits accommodation of large volume change that occurs during charge/discharge cycling of embedded SnO_2 nanoparticles, thereby minimizing electrode destruction from the associated strain. The graphene sheets with high surface area and superior electronic conductivity can build a better conductive network which could facilitate the electron transfer and the diffusion of Li^+ ions inside the GSP during the lithiation and delithiation process. Thus, the enhanced electrochemical performance of the GSP as an anode material in Li-ion battery is obtained. The as-prepared GSP shows a great potential in flexible Li-ion batteries.

2. EXPERIMENTAL SECTION

2.1. Chemical Reagents and Materials. Graphite powder (325 mesh, with purity >99.99%) was obtained from Alfa Aesar. The SnO_2 nanoparticles (particle sizes from 50 to 150 nm, with purity >99.99%) were purchased from Aladdin-Reagent Inc. All other chemicals (purchased from Beijing Chemical Co.,Ltd.) used in this experiment were analytical grade and were used without further purification.

2.2. Preparation of Graphene Oxide (GO) Nanosheets Aqueous Suspension. GO was synthesized from natural graphite powder by the modified Hummer's method as originally presented by Kovtyukhova et al.[46] Then, GO was subjected to dialysis for 7 days to completely remove metal ions and acids. In order to obtain GO nanosheets dispersed in water, the solution after dialysis was sonicated for 1 h with a frequency of 40 kHz (KH-500, Kunshan, Hechuang Ultrasonic Cleaner Inc.). Subsequently, the suspension of GO nanosheets was treated by high-speed centrifugation (10 000 rpm, 5 min) to remove any undispersed solid, and afterward, a brown homogeneous supernatant was collected. The mass concentration of the obtained GO nanosheets aqueous suspension was estimated to be 3.4 mg/mL.

2.3. Preparation of Free-Standing GSP. The free-standing GSP was prepared by a simple filtration method and a subsequent thermal reduction. First, 20 mg of SnO_2 nanoparticles was dispersed into a 50 mL GO (0.8 mg/mL) aqueous suspension by sonication. After that, the GO/SnO_2 nanoparticles suspension was filtrated with a filter membrane (50 mm in diameter, 0.2 μm in pore size) under a positive pressure to produce a GO/SnO_2 nanocomposite paper (GOSP). Subsequently, the GOSP was washed with deionized water and then dried in air. Finally, the flexible free-standing GOSP was peeled off from the filter membrane and thermally reduced in a flow of Ar for 2 h at 400 °C to form a free-standing GSP.

2.4. Characterizations. The structures and compositions of the as-prepared papers were characterized by X-ray powder diffraction (XRD) using a Rigaku Dmax 2200 X-ray diffractometer with Cu Kα radiation (λ = 1.5416 Å). The XRD specimens were prepared by means of pasting the papers on the small slides. The morphology of the as-prepared papers was investigated by JEOL JSM-7001F field-emission scanning electron microscope (FESEM). Transmission

electron microscopy (TEM) and high-resolution transmission electron microscopy (HRTEM) investigations were carried out by a JEOL JEM-2100F microscope. The as-prepared samples were dispersed in ethanol and dropped onto a carbon film supported on a copper grid for the drying process in air. The Raman spectrometer of GOSP and GSP was recorded on a LabRAM HR800 (HORIBA Jobin Yvon) confocal Raman spectrometer, with an excitation laser wavelength of 488 nm.

2.5. Electrochemical Measurements. In order to test the electrochemical performance of the flexible Li-ion anode, flexible free-standing GSP was cut into desired sizes and designed without using other carbon additives, polymer binders, and metal current collectors. By comparison, the SnO_2 nanoparticles electrodes were prepared by mixing 80 wt % active material with 10 wt % carbon black and 10 wt % polyvinylidene fluoride (PVDF) dissolved in *N*-methyl-2-pyrrolidone (NMP) to form a slurry, which was then coated onto a copper foil (current collector), dried at 80 °C for 10 h, and finally pressed under the pressure of 10 MPa. Afterward, CR2016 type coin cells were assembled in a highly pure argon-filled glovebox using the flexible GSP and SnO_2 nanoparticles anode, the metallic lithium counter/reference electrode, a polypropylene separator (Celgard 2400), and an electrolyte of 1 mol/L $LiPF_6$ in ethylene carbonate and diethyl carbonate (EC/DMC, 1:1 vol, Tianjin Jinniu Power Sources Material Co., Ltd. China). Charge−discharge measurements were carried out galvanostatically at a current density of 100 mA/g in the voltage range of 0.005 V~1.5 V using a battery test system (LAND CT2001A model, Wuhan Jinnuo Electronics. Ltd., China). The electrochemical impedance measurements were performed on a CHI660D electrochemical workstation (Shanghai Chenhua Co. Ltd., China) at an AC voltage of 5 mV amplitude in the 100 kHz to 0.01 Hz range.

3. RESULTS AND DISCUSSION

In this work, we adopted a simple filtration method to fabricate the flexible free-standing GOSP, and then, the paper was directly heated in an argon atmosphere to remove oxygen-containing functional groups of GO to form the GSP. The low-, middle- and high-resolution FESEM cross-section images of the paper are shown in Figure 1a,b,c, respectively. From Figure 1a, it can be seen that the fracture edges of the paper exhibits a layered structure through the entire cross-section. SnO_2 nanoparticles and graphene sheets are distributed uniformly into the whole paper which can be seen from Figure 1b. Figure 1c shows the SnO_2 nanoparticles are well embedded into the layers of graphene sheets and the pockets of void spaces are clearly visible which can work as a buffer to prevent the volume expansion and contraction of SnO_2 nanoparticles during the Li^+ insertion/extraction process. Figure 1d,e shows the top view FESEM image of the paper at low and high magnification, respectively. Both the wrinkles and folds of the graphene and the nanosize of the SnO_2 are clearly observed. The presence of wrinkles and folds is the characteristic feature of graphene sheets. From Figure 1e, we can clearly see that the SnO_2 nanoparticles are spread over the graphene sheets surface. SnO_2 nanoparticles can interact with the graphene sheets through physisorption, electrostatic binding, or charge-transfer interactions.[44,47] The graphene sheets with high surface area can help to build a better conductive network which could promote the electron transfer; the graphene sheets with high mechanical flexibility might virtually work as a barrier to avoid the aggregation of SnO_2 nanoparticles and as a buffer to prevent the volume expansion and contraction of SnO_2 nanoparticles during the Li^+ insertion/extraction process. This structure, nanoparticles scattered on flexible graphene nanosheets to form the layered structure, can preserve the internal 3-dimensional network structure of the GSP, which may be beneficial for the electron transfer and accommodation of the strains of Li^+ insertion/extraction to minimize electrode destruction, resulting in excellent Li^+ storage properties. Figure 1f shows the photograph of the as-prepared GOSP, which is free-standing, as being very flexible with high strength. Additionally, it can be prepared into different sizes with various thicknesses and diameters by controlling the amount of solution and the size of filter membrane, which indicates the GSP electrode is very suitable for the application as the anode material in flexible Li-ion batteries.

The representative XRD patterns of GO paper, GOSP, and GSP are shown in Figure 2. For GO paper, a broad diffraction

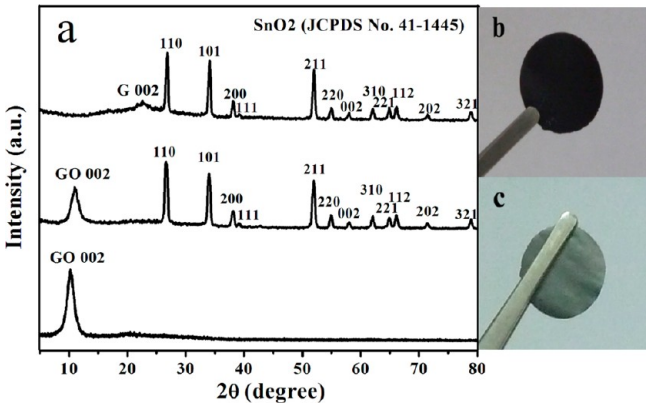

Figure 2. (a) XRD patterns of GO paper (bottom), GOSP (middle), and GSP (top); (b, c) photograph of the paper before (a) and after (b) the thermal reduction process.

peak at 10.3° is a typical peak of GO paper specimen which corresponds to the layer-to-layer distance (*d*-spacing) of about 0.83 nm. This measured distance can be attributed to an approximately one molecule-thick layer of water that is presumably hydrogen-bonded between the GO sheets.[15] For samples of GOSP, the diffraction peaks of the GO and SnO_2 appear simutaneously, indicating the presence of both GO and SnO_2 in the GOSP and implying the GO sheets have been successfully composited with SnO_2 nanoparticles. For the free-standing GSP, the peak of GO is absent, and the appearance of a broadened peak at 24° corresponding to the (002) of graphite indicates the successful reduction of GO to graphene. The SnO_2 nanoparticles are still retained in the paper, as indicated by major diffraction peaks of SnO_2. By incorporating SnO_2 with higher capacity into the graphene paper, the practical capacity of the graphene paper as a Li-ion battery anode can be improved. The photographs of the GOSP and GSP are shown in Figure 2b,c, respectively. Previous research reported that the GO paper was almost black and the graphene paper displayed a shiny metallic luster (bright gray) in the reflection.[15,16] The color of the paper shifted from black (GOSP) to gray (GSP) during the reduction process, which further confirmed the successful reduction of GO to graphene. The paper became brittle after the thermal reduction process. The main reason of this change lies in the fact that the 3-dimensional network structure of the paper is slightly destroyed during the thermal reduction process, which can be clearly seen from the change of the top view FESEM image of the paper from GOSP (Figure S1a,b, Supporting Information) to GSP (Figure 1d,e). Although it became brittle, the GSP was still flexible and could be cut with a metal cutter into free-standing circular disks for the electrochemical testing.

Raman spectroscopy is a powerful tool to characterize carbonaceous materials. The significant structural changes that occurred during the chemical processing from GOSP to GSP are reflected in their Raman spectra (Figure 3). The Raman

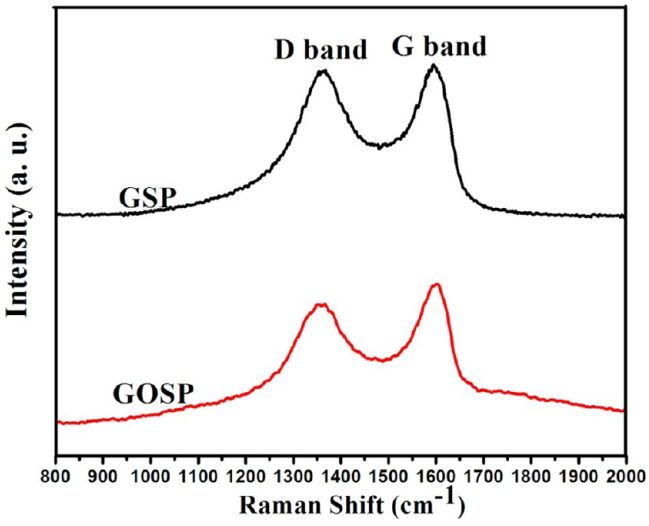

Figure 3. Raman spectra of GOSP and GSP.

spectrum of GOSP contains a G band at 1594.6 cm^{-1} (E2g phonon of C sp2 atoms), owing to the presence of isolated double bonds that resonate at higher frequencies than the G band of graphite. Compared with the Raman spectrum of graphite (Figure S2, Supporting Information), the D band (1363.9 cm^{-1}, κ-point phonons of A1g symmetry) of GO becomes evident, indicating the reduction in size of the in-plane sp^2 domains due to the extensive oxidation.[39,48] Both G band and D band can be also observed in the Raman spectra of GSP, however, with an increased D/G intensity ratio compared to that in GOSP. This change suggests a decrease in the average size of the sp^2 domains upon reduction of the exfoliated GO and can be explained if new graphitic domains are created that are smaller in size than the ones present in GO before reduction but more numerous in number. The change of Raman spectroscopy from GOSP to GSP indicates the successful reduction of GO to graphene. As a result, the GSP are suitable for Li-ion batteries because of the excellent properties of graphene.

The crystalline structure of the GS nanocomposites were analyzed by TEM and HRTEM. Figure 4a shows a low magnification TEM image of the GS nanocomposites; SnO_2 nanoparticles are uniformly distributed on the surface of graphene sheets. Some black areas in Figure 4a are the wrinkles and folds of graphene sheets, which are the characteristic feature of the graphene sheets. A lattice-resolved image of the GS nanocomposites is shown in Figure 4b, showing the lattice spacing of those nanoparticles is 0.33 nm, corresponding to the *d*-spacing of (110) of SnO_2. The stacking layers of graphene nanosheets are 3−5, which can be counted from the number of strips as marked with arrows in Figure 4c. The SnO_2 nanoparticles can be attached on graphene sheets surface firmly even if an ultraphonic process was used to prepare the GS nanocomposites for TEM characterization. The close contact between the SnO_2 nanoparticles and the graphene sheets can minimize the electrical isolation of nanoparticles during battery cycles. The graphene sheets with high surface

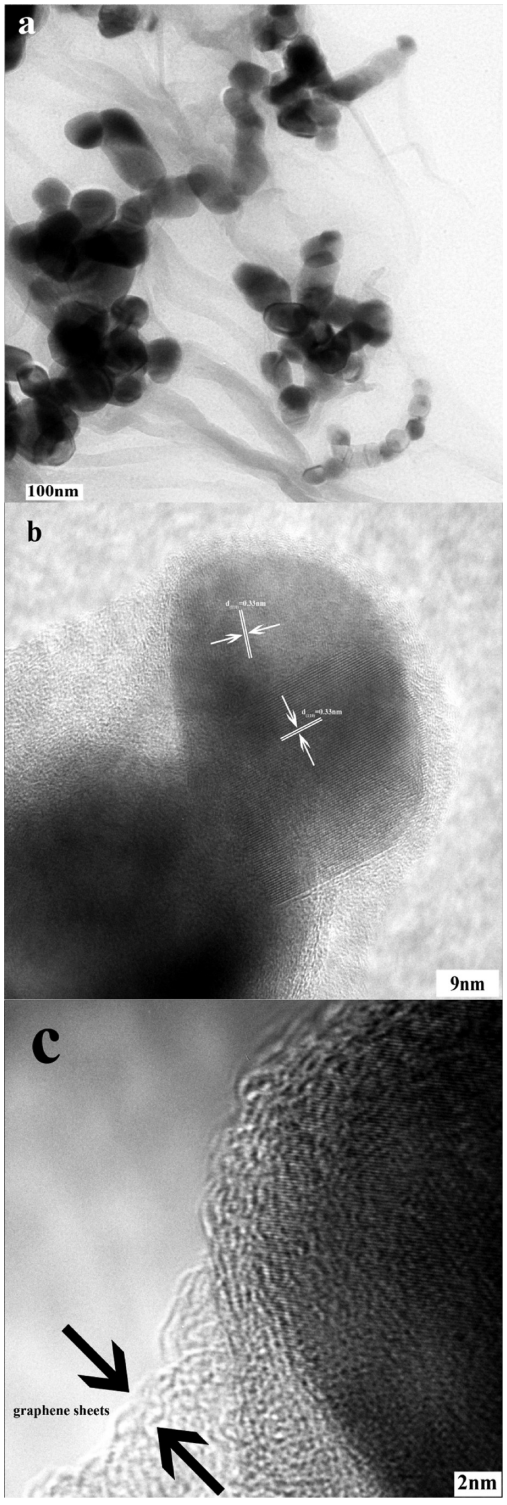

Figure 4. (a) TEM and (b,c) HRTEM images of the GS nanocomposites.

area can build a better conductive network which could facilitate the electron transfer during the lithiation and delithiation process. The high mechanical flexibility of graphene sheets might virtually work as a buffer to prevent the volume expansion and contraction of SnO_2 nanoparticles during Li^+ insertion/extraction and also as a barrier to avoid the aggregation of SnO_2 nanoparticles. These factors would lead to the excellent cycle capability of GSP.

To quantify the mass percentage of SnO_2, the as-prepared GSPs were analyzed by TGA. As shown in the TGA curves (Figure S3, Supporting Information), the GSP shows a rapid mass loss between 450 and 550 °C due to the oxidation of graphene. Therefore, according to the change of weight, it is estimated that the amount of SnO_2 nanoparticles in the nanocomposites is 63%.

To investigate the electrochemical performance of the GSP as an anode for Li-ion batteries, discharge/charge cycling was carried out in the voltage range of 0.005−1.5 V (vs Li/Li^+) at a current density of 100 mA/g under room temperature. The freestanding GSPs were studied using a coin cell design without using other carbon additives, polymer binders, or metal current collectors. For comparison, the SnO_2 nanoparticles were also tested. Figure 5a shows the typical charge/discharge profiles of the nanocomposites paper in the 2nd, 15th, 25th, and 30th cycles. Within the first few cycles, the specific capacity is low because of poor electrolyte wetting of the dense GSP in the absence of polymer binder.[32] The specific capacity gradually increases during the initial 25 cycles as the wetting improves and then levels off basically. The plateau around 0.8 V after the 25th charge curve is longer than the incipient few charge curves, suggesting that the electrochemical reactivity increases due to the improved wetting with increasing cycle numbers. It is very possible that the increasing electrochemical reactivity results in the increase of reversible capacity of GSP. The shape of the profiles does not change significantly during cycling after 25th, indicating the good stability of the nanocomposites paper as an anode for Li-ion batteries.

Figure 5b shows the cyclic performances of GSP and SnO_2 nanoparticles. For GSP and SnO_2 nanoparticles, the discharge capacity dropped rapidly in the first cycle due to the formation of amorphous Li_2O matrix and intense surface reactions with the Li−Sn compounds and the electrolyte solution.[38] In the subsequent charge/discharge cycles, Li^+ was reversibly inserted into Sn as Li_xSn alloys. From the second cycle, the GSP anode showed highly reversible behavior. Within the first few cycles, the GSP exhibited a low reversible capacity because of poor electrolyte wetting of the dense GSP in the absence of polymer binder. However, their specific capacity drastically increased during the initial 25 cycles as the wetting improved and then reached a high specific capacity of 526 mAh/g, as shown in the Figure 5b. After 50 cycles, the discharge capacity still remained 438.5 mAh/g which was about 83.4% retention of the reversible capacity of the 25th. This performance is better than the graphene/SnO_2 nanocomposites film reported previously.[32] Moreover, in the GSP that we studied, the charge and discharge was carried out in a current density of 100 mA/g which was higher than the current density used in the references mentioned above. On the other hand, the SnO_2 nanoparticles electrode exhibited a poor cycle performance; there was a rapid fading of specific capacity due to the severe pulverization, fading rapidly from 663 to 163 mAh/g after 50 cycles with about 24.6% retention of the reversible capacity. Compared with the pure SnO_2 nanparticles, the GSP exhibited superior discharge capacity and cycling performance. In order to clarify the influence of the hybridization on the electrochemical performance of GSP, the theoretical capacity of GSP nanocomposite was estimated by calculating the capacity of a physical mixture of pristine materials (SnO_2 and graphite) according to the theoretical capacities of the SnO_2 (782 mA h g^{-1}) and graphite (372 mA h g^{-1}). On the basis of the weight content (63 wt % SnO_2 and 37 wt % graphene) determined by

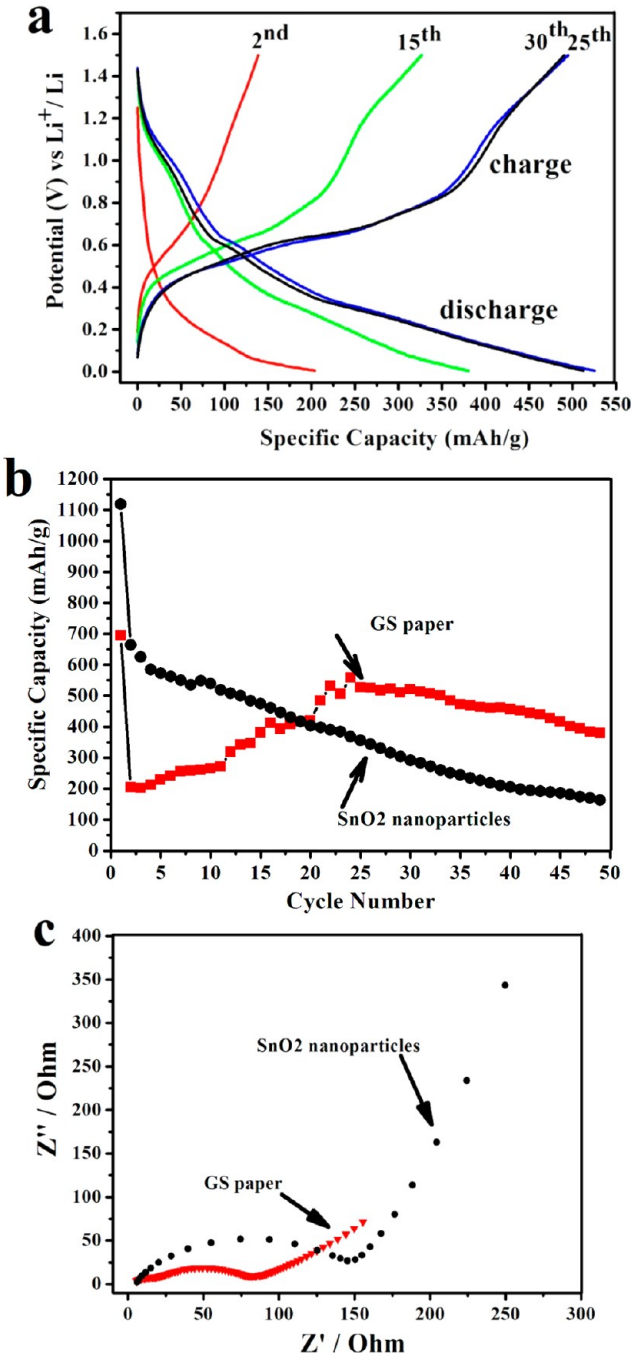

Figure 5. (a) Charge/discharge profile for GSP, (b) the cycle performance of GSP and SnO_2 nanoparticles, and (c) Nyquist plots of GSP and SnO_2 nanoparticles.

TGA, the theoretical capacity of GSP was calculated to be 630 mA h g^{-1}. Despite the considerable drop, the discharge capacity of SnO_2/graphene nanocomposite still remains 69.6% of the theoretical value after 50 cycles. As mentioned before, the SnO_2 nanoparticles have a poor cycle performance and the capacity of reported graphene papers is very low (only around 100 mAh/g)[17,32] The improved performance of GSP observed in our experiments should be attributed to the unique features of the GSP. First, the main reason for the rapid fading of SnO_2 electrode is that the large volume change of the SnO_2 occurs during the charge−discharge cycle, leading to cracking and pulverization of the electrode. A superflexible coating made of

dx.doi.org/10.1021/am301962d | ACS Appl. Mater. Interfaces 2012, 4, 5742−5748

high mechanically flexible graphene sheets covered with the SnO_2 nanocrystals not only provides an elastic buffer space to accommodate the volume changes upon lithium-ion insertion/extraction but also efficiently prevents the aggregation of the nanoparticles and the cracking or crumbling of the electrode material; therefore, a better cycle stability can be obtained. Even though volume expansion still exists, the electrode will not pulverize as the graphene sheets can deform resiliently to accommodate such volume changes. Second, the conductivity of the GSP can be dramatically enhanced because of the presence of the excellent electroconductive graphene. The graphene sheets with high surface area can build a better conductive network which could promote the electron transfer during the lithiation and delithiation process. In the GSP, the electronic transport speed is effectively accelerated compared with the single SnO_2 nanocrystals. Moreover, the graphene sheets provide a continuous conductive path between the SnO_2 nanocrystals, which can reduce the particle−particle interface resistance effectively. The close contact between the SnO_2 nanoparticles and the graphene can also minimize the electrical isolation of nanoparticles during battery cycles. Third, the large specific surface area and the loose stacking of the graphene can give rise to a large contact area between the active material and the electrolyte; the relatively large interlayer spacing between the two graphene sheets provides fast and versatile transport pathways for the electrolyte ions.[49] The above synergetic effects arising from the particular structure of GSP is responsible for the excellent electrochemical performance of the GSP electrode. Meanwhile, the practical capacity of the free-standing graphene paper in Li-ion battery can obviously improve by incorporating an electrochemically active SnO_2 with higher capacity into the graphene paper; the specific capacity of the as-prepared GSP is always higher than the reported graphene paper.

In order to verify the good electrochemical performance of the GSP in comparison with pure SnO_2 nanoparticles, AC impedance spectra measurements were carried out. Figure 5c shows AC impedance spectra of the sample electrodes measured at the open potential of 0.8 V. The typical characteristics of the two Nyquist plots are one semicircle in the high-medium frequency range and a sloping straight line in the low frequency range. The high-frequency semicircle is attributed to SEI film resistance; the spectra in the medium frequency include features that are semicircular in shape and related to electron-transfer resistance, and the inclined straight line corresponds to the lithium-diffusion process within electrodes. From Figure 5c, the diameter of the semicircle for the GSP electrode in the high−medium frequency region is much smaller than that of the pure SnO_2 nanoparticles electrode, which indicates that the GSP has lower contact and electron-transfer resistances when the surface area of both samples is the same for the measurement of the impedance, and implies that the electron transfer inside the GSP is more facile than the SnO_2 nanoparticles. This result shows that graphene in the composites paper not only improves the conductivity of the overall electrode but also largely enhances the electrochemical activity of SnO_2 nanoparticles during the cycle processes.

4. CONCLUSION

In summary, we developed a facile method to prepare flexible free-standing GSP by a simple filtration together with a thermal reduction. Compared with single graphene paper, the GSP shows a higher capacity because of the hybridizing with high capacity SnO_2 nanoparticles. Compared with the pure SnO_2 nanoparticles, the GSP exhibits a better cycling stability because of the hybridizing with excellently flexible and electroconductive graphene. The better Li-storage performance of GSP implies that the as-prepared GSP has great potential for flexible Li-ion batteries. Considering the plentiful properties of both SnO_2 and graphene, the nanocomposites paper could be promisingly applied in many research fields such as ultracapacitors, biosensors, gas sensors, gas storage, and electrochemical analysis in the future. Furthermore, this method may provide a facile, economic, and green strategy for the preparation of other graphene-based nanocomposites paper for different applications.

■ ASSOCIATED CONTENT

Ⓢ Supporting Information

FESEM top view images of the GOSP, The Raman spectra of graphite, and TGA curves of the GSP. This material is available free of charge via the Internet at http://pubs.acs.org.

■ AUTHOR INFORMATION

Corresponding Author

*Tel/Fax: +86-010-82338162. E-mail: lilidong@buaa.edu.cn (L.L.); guolin@buaa.edu.cn (L.G.).

Notes

The authors declare no competing financial interest.

■ ACKNOWLEDGMENTS

This project was financially supported by National Natural Science Foundation of China (11079002 and 51272012) as well as by Specialized Research Fund for the Doctoral Program of Higher Education (20091102110035 and 20111102130006).

■ REFERENCES

(1) Tarascon, J. M.; Armand, M. *Nature* **2001**, *414*, 359−367.
(2) Pushparaj, V. L.; Shaijumon, M. M.; Kumar, A.; Murugesan, S.; Ci, L.; Vajtai, R.; Linhardt, R. J.; Nalamasu, O.; Ajayan, P. M. *Proc. Natl. Acad. Sci. U. S. A.* **2007**, *104*, 13574−13577.
(3) Ban, C. M.; Wu, Z. C.; Gillaspie, D. T.; Chen, L.; Yan, Y. F.; Blackburn, J. L.; Dillon, A. C. *Adv. Mater.* **2010**, *22*, E145−E149.
(4) Jia, X. L.; Yan, C. Z.; Chen, Z.; Wang, R. R.; Zhang, Q.; Guo, L.; Wei, F.; Lu, Y. F. *Chem. Commun.* **2011**, *47*, 9669−9671.
(5) Gwon, H.; Kim, H.-S.; Lee, K. U.; Seo, D.-H.; Park, Y. C.; Lee, Y.-S.; Ahn, B. T.; Kang, K. *Energy Environ. Sci.* **2011**, *4*, 1277−1283.
(6) Novoselov, K. S.; Geim, A. K.; Morozov, S. V.; Jiang, D.; Zhang, Y.; Dubonos, S. V.; Grigorieva, I. V.; Firsov, A. A. *Science* **2004**, *306*, 666−669.
(7) Bolotin, K. I.; Sikes, K. J.; Jiang, Z.; Klima, M.; Fudenberg, G.; Hone, J.; Kim, P.; Stormer, H. L. *Solid State Commun.* **2008**, *146*, 351−355.
(8) Novoselov, K. S.; Geim, A. K.; Morozov, S. V.; Jiang, D.; Katsnelson, M. I.; Grigorieva, I. V.; Dubonos, S. V.; Firsov, A. A. *Nature* **2005**, *438*, 197−200.
(9) Zhang, Y.; Tan, Y.-W.; Stormer, H. L.; Kim, P. *Nature* **2005**, *438*, 201−204.
(10) Lee, C.; Wei, X.; Kysar, J. W.; Hone, J. *Science* **2008**, *321*, 385−388.
(11) Balandin, A. A.; Ghosh, S.; Bao, W.; Calizo, I.; Teweldebrhan, D.; Miao, F.; Lau, C. N. *Nano Lett.* **2008**, *8*, 902−907.
(12) Stankovich, S.; Dikin, D. A.; Piner, R. D.; Kohlhaas, K. A.; Kleinhammes, A.; Jia, Y.; Wu, Y.; Nguyen, S. T.; Ruoff, R. S. *Carbon* **2007**, *45*, 1558−1565.
(13) Li, D.; Müller, M. B.; Gilje, S.; Kaner, R. B.; Wallace, G. G. *Nat. Nanotechnol.* **2008**, *3*, 101−105.
(14) Park, S.; Ruoff, R. S. *Nat. Nanotechnol.* **2009**, *4*, 217−224.

(15) Dikin, D. A.; Stankovich, S.; Zimney, E. J.; Piner, R. D.; Dommett, G. H. B.; Evmenenko, G.; Nguyen, S. T.; Ruoff, R. S. *Nature* **2007**, *448*, 457−460.
(16) Chen, H. Q.; Müller, M. B.; Gilmore, K. J.; Wallace, G. G.; Li, D. *Adv. Mater.* **2008**, *20*, 3557−3561.
(17) Wang, C. Y.; Li, D.; Too, C. O.; Wallace, G. G. *Chem. Mater.* **2009**, *21*, 2604−2606.
(18) Idota, Y.; Kubota, T.; Matsufuji, A.; Maekawa, Y.; Miyasaka, T. *Science* **1997**, *276*, 1395−1397.
(19) Larcher, D.; Beattie, S.; Morcrette, M.; Edstroem, K.; Jumas, J. C.; Tarascon, J. M. *J. Mater. Chem.* **2007**, *17*, 3759−3772.
(20) Wang, H.; Liang, Q. Q.; Wang, W. J.; An, Y. R.; Li, J. H.; Guo, L. *Cryst. Growth Des.* **2011**, *11*, 2942−2947.
(21) Wang, C.; Zhou, Y.; Ge, M. Y.; Xu, X. B.; Zhang, Z. L.; Jiang, J. Z. *J. Am. Chem. Soc.* **2010**, *132*, 46−47.
(22) Wang, Y.; Lee, J. Y.; Zeng, H. C. *Chem. Mater.* **2005**, *17*, 3899−3903.
(23) Wang, H.; Wu, Y. M.; Bai, Y. S.; Zhou, W.; An, Y. R.; Li, J. H.; Guo, L. *J. Mater. Chem.* **2011**, *21*, 10189−10194.
(24) Park, M. S.; Wang, G. X.; Kang, Y. M.; Wexler, D.; Dou, S. X.; Liu, H. K. *Angew. Chem., Int. Ed.* **2007**, *46*, 750−753.
(25) Zhao, N. H.; Wang, G. J.; Huang, Y.; Wang, B.; Yao, B. D.; Wu, Y. P. *Chem. Mater.* **2008**, *20*, 2612−2614.
(26) Kim, J. G.; Nam, S. H.; Lee, S. H.; Choi, S. M.; Kim, W. B. *ACS Appl. Mater. Interfaces* **2011**, *3*, 828−835.
(27) Lou, X. W.; Chen, J. S.; Chen, P.; Archer, L. A. *Chem. Mater.* **2009**, *21*, 2868−2874.
(28) Yang, R.; Zhao, W.; Zheng, J.; Zhang, X. Z.; Li, X. G. *J. Phys. Chem. C* **2010**, *114*, 20272−20276.
(29) Lou, X. W.; Li, C. M.; Archer, A. L. *Adv. Mater.* **2009**, *21*, 2536−2539.
(30) Yuan, L.; Konstantinov, K.; Wang, G. X.; Liu, H. K.; Dou, S. X. *J. Power Sources* **2005**, *146*, 180−184.
(31) Paek, S. M.; Yoo, E.; Honma, I. *Nano Lett.* **2009**, *9*, 72−75.
(32) Wang, D. H.; Kou, R.; Choi, D.; Yang, Z. G.; Nie, Z. M.; Li, J.; Saraf, L. V.; Hu, D. H.; Zhang, J. G.; Graff, G. L.; Liu, J.; Pope, M. A.; Aksay, I. A. *ACS Nano* **2010**, *4*, 1587−1595.
(33) Zhua, X. J.; Zhu, Y. W.; Muralib, S.; Stollerb, M. D.; Ruoff, R. S. *J. Power Sources* **2011**, *196*, 6473−6477.
(34) Ding, S. J.; Luan, D. Y.; Boey, F. Y. C.; Chen, J. S.; Lou, X. W. *Chem. Commun.* **2011**, *47*, 7155−7157.
(35) Zhang, L. S.; Jiang, L. Y.; Yan, H. J.; Wang, W. D.; Wang, W.; Song, W. G.; Guo, Y. G.; Wan, L. J. *J. Mater. Chem.* **2010**, *20*, 5462−5467.
(36) Wang, Z. Y.; Zhang, H.; Li, N.; Shi, Z. J.; Gu, Z. N.; Cao, G. P. *Nano Res.* **2010**, *3*, 748−756.
(37) Kim, H.; Kim, S. W.; Park, Y. U.; Gwon, H.; Seo, D. H.; Kim, Y.; Kang, K. *Nano Res.* **2010**, *3*, 813−821.
(38) Yao, J.; Shen, X. P.; Wang, B.; Liu, H. K.; Wang, G. X. *Electrochem. Commun.* **2009**, *11*, 1849−1852.
(39) Li, Y. M.; Lv, X. J.; Lu, J.; Li, J. H. *J. Phys. Chem. C* **2010**, *114*, 21770−21774.
(40) Zhang, M.; Lei, D. N.; Du, Z. F.; Yin, X. M.; Chen, L. B.; Li, Q. H.; Wang, Y. G.; Wang, T. H. *J. Mater. Chem.* **2011**, *21*, 1673−1676.
(41) Wang, X. Y.; Zhou, X. F.; Yao, K.; Zhang, J. G.; Liu, Z. P. *Carbon* **2011**, *49*, 133−139.
(42) Park, S.-K.; Yu, S.-H.; Pinna, N.; Woo, S.; Jang, B.; Chung, Y.-H.; Cho, Y.-H.; Sung, Y.-E.; Piao, Y. Z. *J. Mater. Chem.* **2012**, *22*, 2520−2525.
(43) Shiva, K.; Rajendra, H. B.; Subrahmanyam, K. S.; Bhattacharyya, A. J.; Rao, C. N. R. *Chem.—Eur. J.* **2012**, *18*, 4489−4494.
(44) Liang, J. F.; Wei, W.; Zhong, D.; Yang, L. Q.; Li, L. D.; Guo, L. *ACS Appl. Mater. Interfaces* **2012**, *4*, 454−459.
(45) Li, X. F.; Meng, X. B.; Liu, J.; Geng, D. S.; Zhang, Y.; Banis, M. N.; Li, Y. L.; Yang, J. L.; Li, R. Y.; Sun, X. L.; Cai, M.; Verbrugge, M. W. *Adv. Funct. Mater.* **2012**, *22*, 1647−1654.
(46) Kovtyukhova, N. I.; Ollivier, P. J.; Martin, B. R.; Mallouk, T. E.; Chizhik, S. A.; Buzaneva, E. V.; Gorchinskiy, A. D. *Chem. Mater.* **1999**, *11*, 771−778.
(47) Li, F. H.; Song, J. F.; Yang, H. F.; Gan, S. Y.; Zhang, Q. X.; Han, D. X.; Ivaska, A.; Niu, L. *Nanotechnology* **2009**, *20*, 455602.
(48) Meng, X. B.; Geng, D. S.; Liu, J. A.; Banis, M. N.; Zhang, Y.; Li, R. Y.; Sun, X. L. *J. Phys. Chem. C* **2010**, *114*, 18330−18337.
(49) Wang, X.; Cao, X. Q.; Bourgeois, L.; Guan, H.; Chen, S. M.; Zhong, Y. T.; Tang, D. M.; Li, H. Q.; Zhai, T. Y.; Li, L.; Bando, Y.; Golberg, D. *Adv. Funct. Mater.* **2012**, *22*, 2682−2690.